

## Fatigue failure monitoring of 316L stainless steel coupons using optical fibre based distributed strain sensing

De Pauw, Ben Dieter; Hinderdael, Michaël; Moonens, Marc; De Baere, Dieter Jens; Geernaert, Thomas; Berghmans, Francis; Guillaume, Patrick

*Published in:*  
Smart Materials and Structures

*DOI:*  
[10.1088/1361-665X/ab32cd](https://doi.org/10.1088/1361-665X/ab32cd)

*Publication date:*  
2019

[Link to publication](#)

### *Citation for published version (APA):*

De Pauw, B. D., Hinderdael, M., Moonens, M., De Baere, D. J., Geernaert, T., Berghmans, F., & Guillaume, P. (2019). Fatigue failure monitoring of 316L stainless steel coupons using optical fibre based distributed strain sensing. *Smart Materials and Structures*, *28*(10), 1-9. [105054]. <https://doi.org/10.1088/1361-665X/ab32cd>

### **Copyright**

No part of this publication may be reproduced or transmitted in any form, without the prior written permission of the author(s) or other rights holders to whom publication rights have been transferred, unless permitted by a license attached to the publication (a Creative Commons license or other), or unless exceptions to copyright law apply.

### **Take down policy**

If you believe that this document infringes your copyright or other rights, please contact [openaccess@vub.be](mailto:openaccess@vub.be), with details of the nature of the infringement. We will investigate the claim and if justified, we will take the appropriate steps.


PAPER

# Fatigue failure monitoring of 316L stainless steel coupons using optical fibre based distributed strain sensing

To cite this article: Ben De Pauw *et al* 2019 *Smart Mater. Struct.* **28** 105054

View the [article online](#) for updates and enhancements.

# Fatigue failure monitoring of 316L stainless steel coupons using optical fibre based distributed strain sensing

Ben De Pauw<sup>1,2</sup> , Michaël Hinderdael<sup>3</sup>, Marc Moonens<sup>3</sup>, Dieter De Baere<sup>3</sup>, Thomas Geernaert<sup>1,2</sup>, Francis Berghmans<sup>1,2</sup> and Patrick Guillaume<sup>3</sup>

<sup>1</sup> Vrije Universiteit Brussel, Department of Applied Physics and Photonics, Brussels Photonics (B-PHOT), Pleinlaan 2, B-1050, Brussels, Belgium

<sup>2</sup> Flanders Make, Oude Diestersebaan 133, B-3920, Lommel, Belgium

<sup>3</sup> Vrije Universiteit Brussel, Department of Mechanical Engineering, Acoustics and Vibration Research Group (AVRG), Pleinlaan 2, B-1050, Brussels, Belgium

E-mail: [ben.de.pauw@vub.be](mailto:ben.de.pauw@vub.be)

Received 14 February 2019, revised 3 July 2019

Accepted for publication 16 July 2019

Published 23 September 2019



CrossMark

## Abstract

We demonstrate the application of optical frequency domain reflectometry to detect, locate and track the propagation of fatigue cracks in simple beam-shaped stainless-steel specimens. To do so we recorded the strain distribution along the entire length of hot rolled and additively manufactured 316L steel specimens with a spatial resolution of 1 mm using an embedded optical fibre, and we evaluated fatigue induced damage under four-point bending load cycles. Our findings are threefold. First, we show that the onset of fatigue damage can be detected using our methodology based on a damage index adapted to optical frequency domain reflectometry measurements, which allows alerting for potential failure. We also show that our optical fibre mounting and embedding technique enables the fibre to survive critical failure of the steel specimen. In addition, we obtain strain profile measurements with a spatial resolution that allows linking the strain distribution with imperfections in the four-point bending set-up.

Keywords: metal fatigue, distributed strain sensing, optical fibre sensors, OFDR

(Some figures may appear in colour only in the online journal)

## 1. Introduction

In metallic structures, the most important and most common form of damage stems from material fatigue, which is associated with localised and progressive damage resulting from cyclic loading at load levels that are significantly lower than the failure load [1–4]. Fatigue failure occurs following the initiation of microscopic cracks in a structural component, typically (but not exclusively) at locations of high stress, and the growth and propagation of these cracks leading to the rupture of the component [5, 6]. Early detection of growing fatigue cracks is therefore important to initiate corrective actions with the aim to avoid failure of the component [7].

Non-destructive testing (NDT) inspections can be conducted at regular time intervals to detect crack growth. State-

of-the-art NDT methods to monitor fatigue can involve local strain or displacement measurements at the surface of the component or rely on indirect measurements such as vibrations and modal analyses [1, 4, 7–11]. The former require physical access to an adequate (i.e. smooth and sufficiently large) area for mounting strain gauges near the locations of anticipated high stress or need optical access in the case of imaging techniques, which cannot always be guaranteed. Furthermore, point-based sensors such as crack propagation gauges or electrical strain gauges are unable to provide structural information about other (not instrumented) locations [1, 4, 7, 12]. On the other hand, full-field imaging techniques only provide information at the surface of the component under test [8, 9, 13]. In the case of indirect measurements, it is very challenging to relate an observed

response to the occurrence and location of fatigue damage. In most cases, such a technique relies on the development of a model to which the observed situation can be compared to [4, 7, 11, 14–17]. Consequently, the reliability of these methods essentially depend on the quality of the models. Note that other NDT methods can be applied to monitor fatigue such as technologies relying on ultrasound, eddy currents, liquid penetrants, x-rays, .... These techniques however are outside the scope of this paper.

Advancements in steel manufacturing techniques, such as additive manufacturing, now allow for the fabrication of thinner and more intricate structural components. This not only complicates the installation of surface mounted sensors, but also increases the number of critical areas where high stress concentrations can occur, which also calls for implementing more adequate NDT techniques to monitor and to detect the occurrence of fatigue damage [18–21].

In this paper, we address these issues and we attempt to overcome important drawbacks of conventional fatigue damage methods by demonstrating an alternative sensing solution that relies on an optical fibre to determine the distributed strain along the fibre and that allows monitoring the occurrence and evolution of fatigue damage. The technique is based on so-called ‘Optical Frequency Domain Reflectometry’ (OFDR) and allows recording changes in the amount of light scattered inside an optical fibre resulting from changes in the local (relative) strain level [22, 23]. As a proof-of-principle, we apply this method to well-understood 316L stainless steel beam-shaped specimens and we show that it allows recording the internal strain distribution of the specimen with a spatial resolution of 1mm and a sensitivity of approximately 1 micro-strain. To the best of our knowledge these conditions have not been demonstrated to monitor fatigue in metallic components. To further illustrate the potential of our approach, we recorded the strain distribution internally in the steel specimen in view of anticipated developments in additive manufacturing technology [24–26].

The remainder of this paper is structured as follows. Section 2 describes the manufacturing of the test specimens and discusses the experimental test set-up. We explain the principle of distributed strain sensing using OFDR and how we applied this to reconstruct the strain profile in a steel specimen subjected to four point bending with the aim to validate the test procedure. We also deal with two approaches to initiate fatigue damage in the tested specimens. We discuss the experimental results and explain how these relate to the presence, location and growth of fatigue cracks in section 3. Section 4 closes our paper with a summary and conclusions.

## 2. Experimental method and set-up

### 2.1. Materials and experimental set-up

We manufactured three beam-shaped test specimens in 316L stainless steel of which two specimens were milled from a block of hot rolled material and a third specimen was produced from a block of laser based ‘Directed Energy

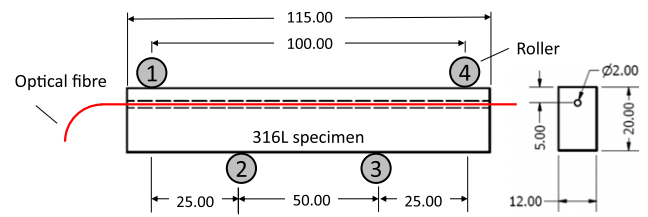


**Figure 1.** Schematic representation of the four point bending set-up and fatigue test specimen with an integrated optical fibre fixed inside a capillary. Dimensions are in millimetres.

Deposition’ (DED) [27] manufactured material. The latter is a metal additive manufacturing (AM) technique, which we considered in view of illustrating the applicability of our concept to such recent manufacturing techniques that results in very different failure loads although the material is exactly the same [28]. We used one specimen to validate the experimental set-up as described in section 2.3 whilst we tested the remaining two specimens under fatigue loads (section 3).

All 3 specimens had overall dimensions of 12 mm × 20 mm × 115 mm. Generally speaking, the preferred location for attaching fatigue sensors that rely on strain measurements is the surface of the component where the highest strains are expected. These high strains however, which are expected to cause fatigue damage in the steel component, are also likely to damage said sensors. In addition, a complex engineering component can have multiple surfaces where critical strain levels are expected. It would hence not be very practical or cost-effective to instrument every critical area of the component since the presence of a multitude of surface mounted sensors each requiring some sort of wiring, which in its turn also significantly impacts the handling of the component. Therefore, we opted to demonstrate the use of an embedded optical fibre in the steel specimen. To do so, the 3 steel specimen were equipped with an integrated capillary in which the optical fibre could be embedded, as schematically illustrated in figure 1. This straight 2 mm diameter capillary was drilled using deep-gun drilling through the entire test specimen. Note also that the embedding of the optical fibre appears compatible with the anticipated developments in AM as for example the DED technique could allow incorporating the capillary and even the optical fibre during the actual manufacturing of the sample [24–26].

To install the optical fibre, we first pressure-filled the capillary, from the bottom up, with a two-component epoxy adhesive (HBM X120). The selected adhesive exhibits very limited out-gassing, cures at room temperature after mixing and does not lead to curing-induced non-uniform stress that would be transferred to the fibre, making the epoxy very suitable for our application. Subsequently, we inserted a pre-wetted optical fibre inside the capillary and ensured that the fibre was centred and aligned. The selected optical fibre was a mechanically strong optical fibre assembly consisting of a Ge-doped single mode fibre (125 μm diameter and numerical

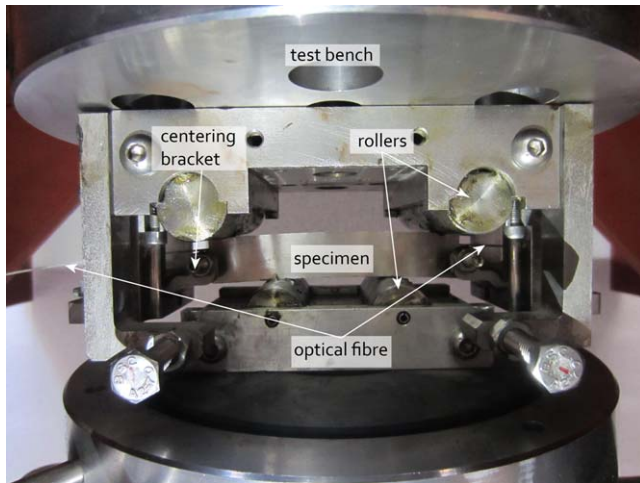


**Figure 2.** Photograph of the four-point bending fatigue test bench with installed specimen and integrated optical fibre.

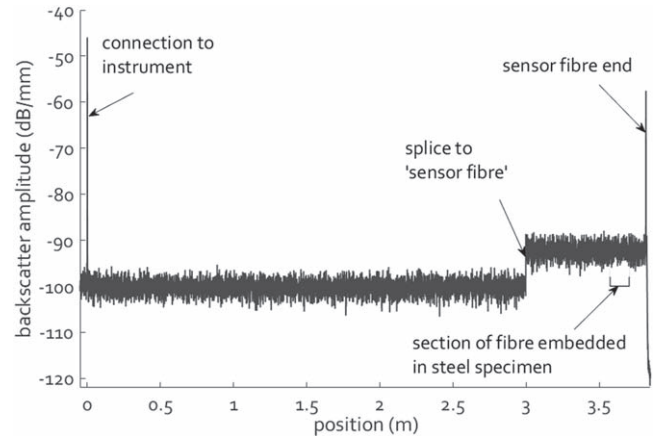
aperture of 0.26) equipped with a glass-fibre reinforced polymer coating with an outer diameter of 1 mm.

Figure 2 shows a photograph of the four-point bending fatigue test set-up. The supports consisted of four steel rollers. The top rollers are actuated, whilst the bottom rollers remain fixed. Centring brackets ensured that the specimen were properly aligned in the plane perpendicular to the actuation axis. The diameter of the roller supports was 25 mm. We set the fatigue loading to be a sinusoidal cyclic load at 15 Hz with a stress ratio (*R* ratio) of 0.1. The mean load was different for each experiment and ranged between 12.4 and 24 kN. For each of the tested specimens however, we followed different procedures to promote the occurrence and propagation of a fatigue crack under four-point bending as detailed in the subsequent sections.

The capillary is oriented perpendicularly to the principal stress direction for the specimen in the 4-point bending setup. The cross-section of the specimen is uniform across its entire length. The capillary does not introduce local stress concentrations, but only leads to an overall increase of the stress since the load is distributed over a smaller, but uniform, cross-section. It has been shown that the capillary does not act as an initiation site for fatigue damage and that the fatigue properties of the specimen remain unaltered when including such capillaries [29, 30]. A summary of fatigue tests of specimen with and without capillary is shown in table 1 in [31].

## 2.2. Distributed strain sensing methodology using OFDR

Optical fibre based sensors are already applied to monitor fatigue in components as for example in [32–34]. However and to the best of our knowledge, no published work exists where distributed strain measurements (with a spatial resolution of 1mm and a sensitivity of approximately 1 micro-strain) have been applied inside steel structures to monitor fatigue. Our methodology described in this paper builds on so-called ‘Optical Frequency Domain Reflectometry’ or OFDR which relies on the full scalar response of the optical backscatter in an optical fibre [22, 23]. The backscatter



**Figure 3.** Typical response of the optical fibre using the OFDR technique which relies on the scattering losses at every position in the optical fibre that are inherent to the fibre. Local changes in the scattering losses can be linked to local temperature or strain changes.

originates from random (small) fluctuations in the refractive index profile along the fibre length. The signal is therefore inherent to the optical fibre under test and depends on the position along the optical fibre. Such a backscatter trace measurement is sometimes referred to as the ‘fingerprint’ of the fibre. Changes in environmental parameters such as temperature and strain can affect the physical length and local index of refraction of the fibre and thus also modify the fingerprint of the fibre. The resulting changes in the backscatter are recorded as temporal shifts resulting from time-of-flight measurements of light pulses (or spectral shifts in the frequency domain) and can be linked to local changes in temperature, strain, etc with a millimetre-scale spatial resolution over tens to hundreds of meters of optical fibre [35]. Cross-correlating two recorded fingerprints determines the size of the temporal shifts. The achievable spatial resolution depends on the noise in the cross-correlation: lower signal noise corresponds to an improved spatial resolution. Note that any two fingerprints can be correlated to determine the local temperature or strain difference between the two records in the tested optical fibre. The obtained strain and temperature resolution are typically on the order of a few micro-strain ( $\mu\epsilon$ ) and a few tenths of a degree. These specifications surpass typical measurement techniques used for fatigue monitoring relying on strain measurements [8, 9, 12]. OFDR is typically applied as a (small-sized) network analysis tool [36, 37], for distributed temperature [38–41] or strain sensing [41–43].

Figure 3 shows an example of such a fingerprint for the fibre used in the fatigue experiments. In our experiments we used a Luna Innovations OBR 4400 [35]. The fibres had a length of about 3.7 m consisting of a 3.0 m long optical fibre and a 0.7 m section of Ge-doped single mode fibre with 1 mm outer diameter to increase stiffness and to avoid micro-bends that affect the fingerprint. To maximize the signal-to-noise ratio and to obtain the mentioned spatial resolution at the relevant section of the optical fibre, sources of noise such as Fresnel-type reflections at the fibre end-faces should be avoided or reduced as much as possible. In figure 3 such reflections can be found, as expected, at the entrance of the

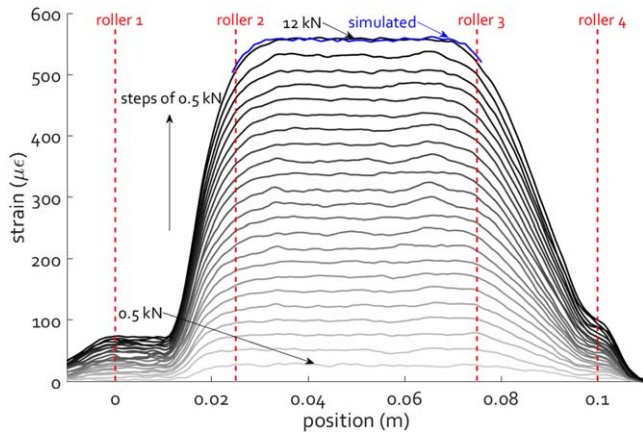


**Figure 4.** Experimentally obtained strain distribution curves (in grey) of a pristine steel (wrought) specimen in the four point bending set-up under different load amplitudes as well as a numerical simulated curve (in blue) for a load of 12 kN. The spatial resolution was 1 mm.

source and detector (at 0 m) and at the free end-face of the fibre (at 3.7 m). To reduce the reflections from the free end-face of the optical fibre (at 3.7 m), we dipped it in so-called index-matching gel. Such a substance has a refractive index close to the refractive index of the light guiding part of the optical fibre and allows most of the light guided in the optical fibre to escape instead of being reflected back into the fibre. At the other extremity (at 0 m), good coupling with minimal reflections is ensured owing to a FC/APC type connection (typical return loss of  $-55$  dB) and a cleaned, correctly mated connector.

### 2.3. Validation of experimental set-up

Prior to conducting the fatigue experiments, we validated our experimental set-up including the mounting of the optical fibre in a reference specimen, which was one of the three fabricated specimens. Once installed in the four-point bending test rig, we statically loaded a wrought (hot-rolled) steel specimens and determined the strain distribution inside the specimen using the OFDR technique. First a small load of 500 N was applied to the specimen and the corresponding backscatter profile was used as reference. The load on the specimen was subsequently increased in steps of 500 N up to 12 kN. At each step, the updated backscatter profile was correlated this to the reference (at 500 N) to obtain the strain difference distribution in the steel specimen. Recall that the high signal-to-noise ratio allows recording the strain distribution with a spatial resolution of 1 mm. Figure 4 shows the resulting relative strain distributions. It is clear from the figure that the strain between the two inner rollers is maximum and effectively constant. Consequently, fatigue cracks are expected to nucleate and grow in this region. The strain grows linearly between the outer and inner rollers. All these observations are in line with what is expected for a four point bending set-up [44] which essentially validates the set-up and the measurement method. Beyond the left-hand outer roller, the alignment pin of the fibre (used to centre the fibre in the capillary) retains the strain over a distance of approximately

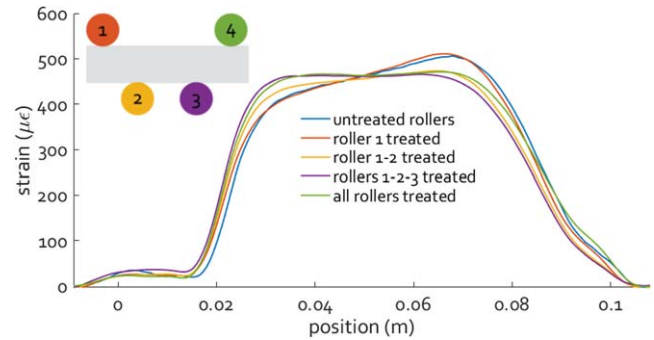


**Figure 5.** The OFDR measurement technique allowed evaluating the quality of the roller supports. Subsequent cleaning and lubrication of the rollers altered the stress distribution inside the specimen, finally resulting in a constant strain distribution between the two central rollers.

1 cm. In addition, the maximum strain observed between the two inner rollers was linear with the applied load (up until the highest tested load of 12 kN in the described situation). The measured maximum tensile strain for the 12 kN case (i.e. a difference of 11.5 kN) equals  $557.8 \mu\epsilon \pm 1.4 \mu\epsilon$ .

We compared the observed maximum tensile strain with a numerically calculated value. To do so, we have built a finite element model in Abaqus FEA in which the optical fibre was modelled as ‘perfectly embedded’ which means that continuous boundaries were considered. The rollers were defined as ‘stiff’ and thus no deformation of the rollers was allowed. The tangential friction coefficient was empirically determined and equal to 0.02. The result of the simulations between the central rollers for 12 kN is shown in blue in figure 4 and agrees well with the experimentally obtained values. Moreover, the calculated maximum tensile strain was  $556.8 \mu\epsilon$  which is within the measurement uncertainty of the experimentally obtained value.

Recall that the obtained backscatter profiles depend on the applied strain and temperature along the optical fibre. However, any part of the optical fibre that is not embedded in the steel specimen does not experience strain and thus the backscatter profile at that location will only be sensitive to temperature. We used this information to compensate for temperature fluctuations, where required, in the remainder of this paper. The observed temperature fluctuations during our experimental campaigns were approximately 2–3 K.

An extra feature of the measurement of the shape of the strain distribution curves between the rollers is that this allows evaluating the position of the test specimen and the roller supports of the set-up. In particular, the strain experienced by the specimen should reach a plateau and a maximum in the region between the two inner rollers. However, if one of the rollers is not adequately cleaned and lubricated, the strain measured between the inner rollers will exhibit a slope. To illustrate this, we mounted the reference specimen with embedded optical fibre in the test set-up using 4 rollers that were used in a previous fatigue experiment and showed traces of wear. The blue curve in figure 5 shows the strain distribution that was initially obtained. The presence of a clear slope (with a maximum on the right-hand side) demonstrates

that the rollers need to be cleaned (or even replaced) and lubricated. The four rollers were treated consecutively and the altered strain distribution after each treatment was recorded. Figure 4 shows the corresponding curves. Before the treatment of the rollers, the stress level in the region between the inner rollers showed an important stress difference of  $\pm 12\%$  as compared to the nominal value. Such differences may be sufficient to favour fatigue initiation at the location of highest stress. To validate fatigue test results, it is therefore important to check the stress distribution obtained during practical testing rather than conduct single point measurements. We conclude from figure 5 that the treatment of rollers 2 and 3, i.e. the two inner (or bottom) rollers, yield the most significant effect. After treatment of all rollers, the region of maximum strain between the two inner rollers was constant. This evidences that paying attention to the lubrication of the supports is crucial in such experiments. The overall conclusion of this section is that the distributed strain sensing methodology relying on an embedded optical fibre is a suitable technique to reconstruct the stress profile inside the test specimen and that it can be used to verify whether the test set-up is correctly maintained and operated.

### 3. Monitoring of fatigue damage in steel specimen

In this section we deal with the application of the distributed strain sensing methodology described in the previous section to monitor the presence and propagation of fatigue damage in the 316L stainless steel specimen as proof-of-principle. The first test focuses on a pre-cracked specimen for which the location of the fatigue crack was not known. In a second experiment we evaluated a notched pristine (i.e. not pre-cracked) specimen in order to detect the presence and follow the growth of a fatigue crack.

#### 3.1. Specimen with invisible crack

To validate the observation of fatigue damage using the optical fibre based distributed sensing technique, we subjected a specimen (fabricated using DED) to fatigue cycles, prior to the OFDR measurements, and halted the experiment as soon as damage was observed by monitoring the internal air pressure in the pristine capillary (i.e. before the optical fibre is mounted). The internal pressure was initially reduced in the capillary to create a partial vacuum. This pressure returned to atmospheric pressure as soon as a fatigue induced crack has propagated from the surface up to the capillary. We validated this technique in previous work and more details can be found in [31]. Note that no macroscopic fatigue cracks were visible when the pressure had normalized and thus that the location of damage was unknown *a priori*. We then mounted the optical fibre in the capillary (as described earlier) of the invisibly damaged specimen and evaluated the strain distribution over the optical fibre inside the specimen for different *static* loads initially. Figure 6 shows the measured strain distribution with a spatial resolution of 1mm when an additional load of 10 kN was applied compared to the

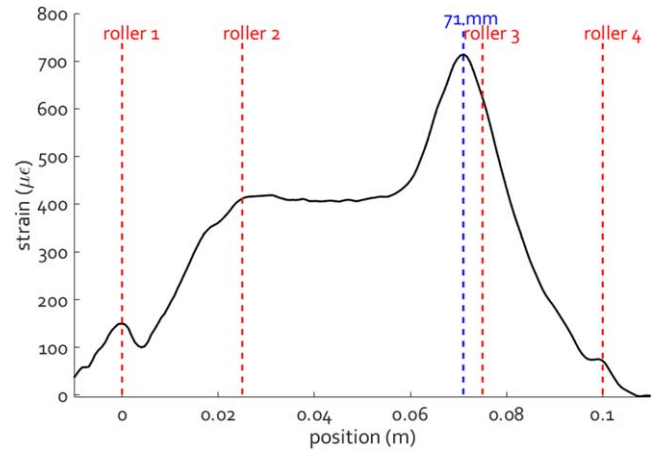


**Figure 6.** The strain distribution observed in the pre-damaged specimen when a static load of 10 kN was applied. We expect the location of high strain concentration at 71 mm to correspond to that of the fatigue crack.

reference ‘fingerprint’ at 500 N. The strain distribution expected from a four point bending set-up remains unaltered, except at a position around 71 mm where a clear strain concentration (i.e. strain hardening) can be observed. As mentioned, the specimen was pre-damaged with the fatigue crack having propagated up to the capillary which leads to a stress concentration at the crack location that can be clearly observed with the optical fibre. We therefore believe that the high strain concentration at 71 mm reveals the location of the fatigue crack. This hypothesis is a conventional approach in case of e.g. imaging techniques (as for example in [9]), supporting to the applicability of our methodology. Note that the fatigue crack must have propagated over the distance between the top surface of the specimen and the capillary, yielding a fatigue crack length of at least 5 mm and a width that is too small to be visualized without microscopes.

Note that the four-point bending of the beam-shaped specimens guarantees that a fatigue crack will propagate parallel with the direction of the load and thus towards the location of the optical fibre. This renders the optical fibre particularly sensitive to fatigue damage. For many applications that leverage on bending, a similar situation can be considered. For other applications however, the location and path of the capillary and thus the optical fibre might require more deliberation.

The specimen was subsequently subjected to fatigue cycles to evaluate the growth of the fatigue crack and to confirm visually the location of the damage. The mean load on the specimen was 24 kN with a stress ratio (R ratio) of 0.1 [28]. We interrupted cycling every 1000 cycles and recorded the backscatter profile at 24 kN to evaluate the change in the strain distribution by correlating the profile with the last recorded profile rather than the initially measured one. Note that correlating with the initial profile is the conventional approach used in OFDR analyses. In our case this would lead to erroneous results due to excessive and localized temporal shifts corresponding to large strains. Correlating with the last recorded profile instead proved to be very suitable for the

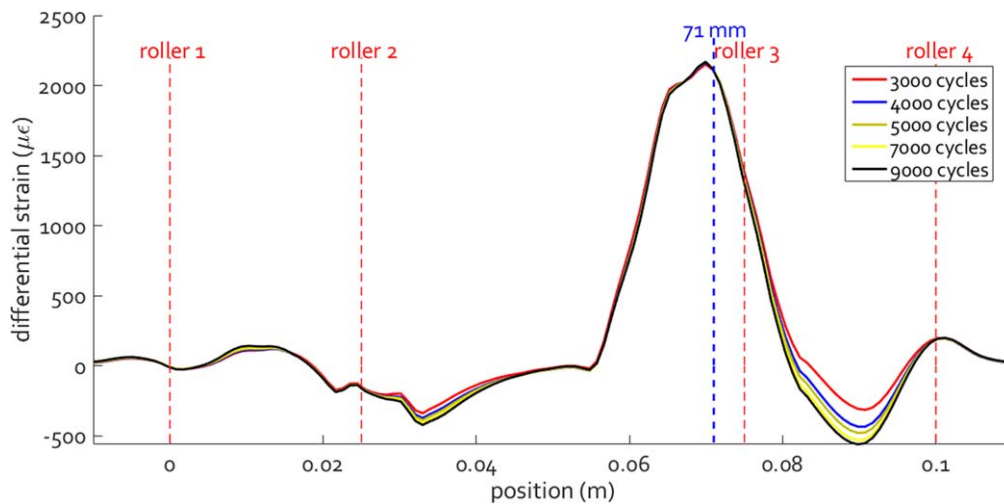


**Figure 7.** The difference in strain compared to the distribution in figure 6 obtained approximately every 1000 fatigue cycles clearly shows the location of the damage at approximately 71 mm. We believe that the observed increase of compression in the vicinity of the damage indicates the growth of the width of the fatigue crack.

current application as the incremental temporal shifts are significantly smaller. The total temporal shift and corresponding strain can then be calculated cumulatively. In addition, relying on the strain difference between consecutive measurements allows (partially) eliminating the impact on the measurements of more gradually occurring effects such as wear of the roller supports (illustrated in the previous section), whilst emphasizing the impact of more sudden strain changes that stem from fatigue damage. We established that growth of the fatigue crack corresponds to a higher stress concentration observed by the optical fibre as illustrated in figure 7 which shows five cumulative strain distributions for different amounts of fatigue cycles. The displayed strain distributions correspond to the total difference compared to that shown in figure 6. The highest change in strain is found close to 71 mm which coincides with the location of the fatigue crack. We observed increasing compression in the vicinity of the crack with an increasing amount of strain cycles and believe that this corresponds to an increase in the fatigue crack width as the crack had propagated already from the surface to the capillary and optical fibre.

After approximately 10 000 cycles, the fatigue crack had grown to a visible fracture as shown in figure 8. The location of the fracture corresponded to the anticipated location at 71 mm. Note that upon fracture (and continued loading) the optical fibre remained intact and still allowed recording the backscatter profile (see figure 9). This indicates that our fibre assembly and mounting method allows for continued measurements at other locations in the specimen even when the latter failed.

### 3.2. Pristine specimen with notch

The previous section demonstrated the potential of our distributed sensing methodology to locate otherwise invisible fatigue cracks and monitor their propagation. In view of practical structural health monitoring applications, we extended our experiments towards monitoring fatigue damage on a



**Figure 8.** The location of the fatigue crack is measured to be 71 mm away from outer roller 1.

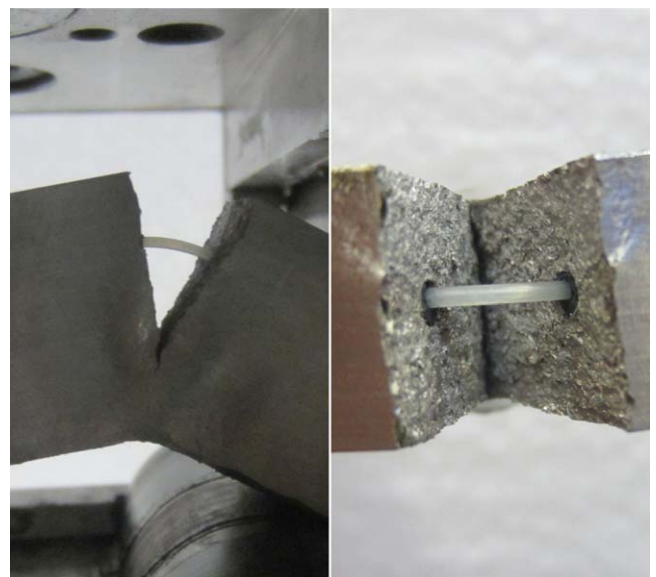


**Figure 9.** Upon further fracturing of the steel specimen, the embedded optical fibre was revealed and proved to be intact.



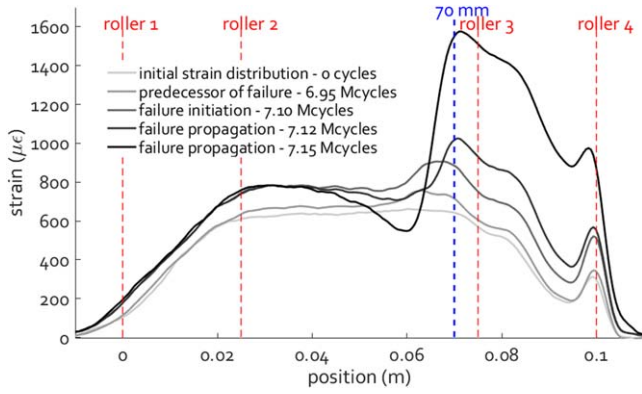


**Figure 10.** Evolution of the strain distribution in the steel specimen obtained during the blind test. The fatigue-induced crack formation, propagation and location are clearly observable. We visually determined location of the damage at 70 mm, indicated in the figure in blue.

pristine (i.e. not pre-cracked wrought) specimen. To be able to validate the location of damage in the specimen, a small triangular notch was created of approximately 2 mm in width at one of the top edges (tensile stressed) of the specimen. The existence of the notch leads to higher local stress concentrations during loading, which promote the occurrence of fatigue damage. The fatigue cycles were applied to the specimen with a mean load of 12.4 kN and a stress ratio of 0.1. A smaller mean load was used compared to the previous section due to the anticipated difference in failure load between the wrought specimen and the DED specimen [28]. We interrupted fatigue loading after every 5000 cycles to record the backscatter profile of the optical fibre embedded in the steel specimen at 12.4 kN.

Figure 10 shows the strain distribution at 5 different instances during the fatigue test. We determined the strain distributions by comparing a 500 N reference to a static load of 12.4 kN. Initially, at 0 fatigue cycles, the strain distribution corresponds to the curve expected in a four point bending set-up. Slight wear of the four-point bending rollers may be responsible for the small slope at the maximum strain plateau. Up to 6.95 Mcycles, the strain distribution remained essentially constant, except for a small amount of strain hardening. To further facilitate the occurrence of fatigue damage, the size of the notch was approximately doubled on one of the top edges of the specimen after 6.95 Mcycles and the roller supports were rotated. At 7.10 Mcycles i.e. 150 kcycles later, a small strain concentration appeared similar to that observed in the specimen tested in the previous section albeit with a smaller strain amplitude. This indicates that fatigue induced cracks are present in the specimen and are growing. The location of this fatigue damage appeared at around 70 mm. In the two subsequent curves at 7.12 and 7.15 Mcycles, the size of the damage grew quickly until failure of the steel specimen. The rupture location exactly corresponds to the anticipated location i.e. the location of the notch and the location of the precursor of damage in the strain distribution curves.

To avoid the need for analysing the entire strain distribution, we looked into the possibility of defining a single

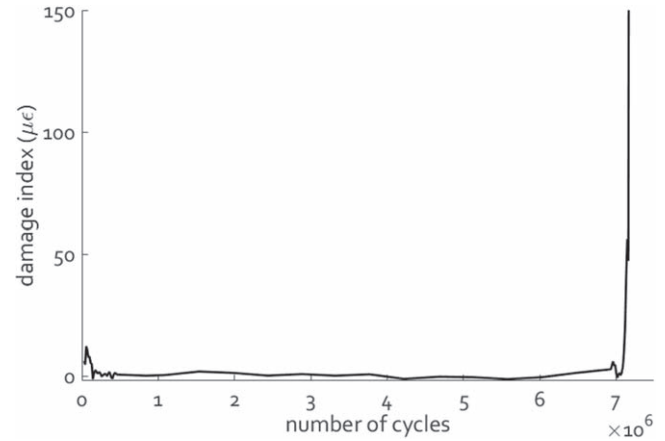


**Figure 11.** Evaluation of the damage index as a function of the number of applied fatigue cycles. Shortly after 7.10 Mcycles, fatigue damage began to propagate.

parameter or figure of merit that can be calculated and used to alert a user for the presence of fatigue damage based on an OFDR measurement. We therefore defined a damage index (DI) that can be calculated from the differential strain distributions i.e. the correlation of two consecutive backscatter profiles to determine the local change in strain. This also allows avoiding gradual changes resulting from the degradation of the roller supports and eliminating the need to calculate the cumulative strain from all the previously measured differential strain distributions. We define this DI as,

$$DI \equiv \frac{1}{A * L} \sum_{k=1}^N (|\Delta \epsilon_k| * l_s), \quad (1)$$

where  $\Delta \epsilon_k$  is the differential strain determined from two consecutive backscatter profiles at position  $k$  with  $N l_s \equiv L$  the total analysed length of the optical fibre, which equals 140 mm.  $l_s$  thus corresponds to the 1 mm spatial resolution of the measurement. This suggested DI is particularly useful to evaluate a section of uniform strain such as the area between the inner rollers in the four-point bending set-up. In a different application, a different DI may be more suitable. Furthermore and depending on the application, a user can define an adequate threshold for the DI and normalize using  $A$  to enable real-time damage monitoring and potential failure prediction. In our case for example, the DI could be normalized with respect to the observed strain at the plateau. Such a normalization would imply that gradual changes in load conditions (e.g. when the applied load is not constant over time) or temperature fluctuations that occur on a time-scale longer than the time between two measurements are rendered negligible. Since the applied loads during measurements were the same during the entire test campaign and the observed temperature changes were small, we nevertheless opted not to normalize the DI in this paper and we kept  $A = 1$ . Figure 11 shows the DI, calculated according to equation (1) of the tested specimen as a function of the number of applied fatigue cycles. The measurements up to around 130000 fatigue cycles show that the DI is between 5 and 12  $\mu\epsilon$ . We believe that this stems from the plastic deformation that occurs at the location of the



**Figure 12.** After approximately 7.20 Mcycles, the fatigue crack was clearly visible and located at 70 mm from outer roller 1.

rollers as these tend to compress and indent the specimen during the first cycles. Up to about 6.95 Mcycles, the DI remained close to  $0\text{--}3\ \mu\epsilon$ . As mentioned earlier, the occurrence of fatigue damage was facilitated by increasing the size of the notch on one of the top edges of the specimen after 6.95 Mcycles and rotated the roller supports. The latter led to a small increase in the DI to about  $8\text{--}9\ \mu\epsilon$  which again normalized after approximately 100 000 cycles. Close to 7.10 Mcycles, shortly after the modification of the notch, the DI began to increase and continued to increase during more than  $1 \times 10^5$  cycles until the test specimen failed. For the sake of legibility, the vertical axis of figure 11 is limited to  $150\ \mu\epsilon$ , but note that the DI continued to increase far beyond  $1000\ \mu\epsilon$ . This shows that such DI can be a clear indicator for damage detection based on OFDR measurements.

Figure 12 shows the fractured specimen. Note that the optical fibre again remained intact after more than 7.20 Mcycles, confirming the robustness of the applied mounting method and the ability to continue measurements across the rest of the specimen.

#### 4. Summary and conclusions

We studied the detection, location and propagation of fatigue induced damage in 316L stainless steel specimens using distributed optical fibre based strain sensing (OFDR). We mounted the optical fibres inside a capillary within these specimens and we determined the strain distribution in the specimen along the entire length of the optical fibre (i.e. without defining critical locations). When subjected to static loads in a four-point bending set-up, we observed that the measured strain distribution agrees well with the theoretically calculated value. The obtained spatial resolution was 1 mm while the strain sensitivity was approximately  $1\ \mu\epsilon$ .

We applied fatigue cycles to two 316L test specimens and we monitored the strain distribution at regular intervals. For both specimens, our distributed strain sensing methodology allowed detecting the presence, location and propagation of fatigue induced damage. In addition, we illustrated that the difference in the strain distribution between consecutive measurements can handle the large observed strain. In both tests, the optical fibres remained intact in spite of the

fracture of the specimen and allowed for continued strain measurements at other locations in the specimen. Finally, we have shown that the strain measurements even allow linking the strain distribution with the degradation of the lubrication of the four-point bending supporting rollers or by extension with other imperfections in the test set-up.

The above indicates that our fatigue detection methodology potentially allows avoiding typical drawbacks linked to conventional fatigue monitoring techniques. Furthermore, this methodology can be scaled to accommodate much longer optical fibre lengths (provided the fibre can be mounted), potentially enabling structural health monitoring of real-world engineering components and systems rather than small-sized specimens only.

#### Acknowledgments

Ben De Pauw and Michaël Hinderdael are post-doctoral fellows of the Research Foundation Flanders (FWO). B-PHOT and AVRГ acknowledge the Vrije Universiteit Brussel's Methusalem programme as well as the Hercules programme of the FWO. This work was also partially performed as part of the Innovative Training Network FINESSE, funded by the European Union's Horizon 2020 research and innovation program under the Marie Skłodowska-Curie Action grant agreement no. 722509.

#### ORCID iDs

Ben De Pauw  <https://orcid.org/0000-0002-9606-0483>

#### References

- [1] Schijve J 2003 Fatigue of structures and materials in the 20th century and the state of the art *Int. J. Fatigue* **25** 679–702
- [2] Papadopoulos I V, Davoli P, Gorla C, Filippini M and Bernasconi A 1997 A comparative study of multiaxial high-cycle fatigue criteria for metals *Int. J. Fatigue* **19** 219–35
- [3] Carpinteri A and Spagnoli A 2001 Multiaxial high-cycle fatigue criterion for hard metals *Int. J. Fatigue* **23** 135–45
- [4] Stephens R I, Fatemi A, Stephens R R and Fuchs H O 2000 *Metal Fatigue in Engineering* (New York: Wiley) 9780471510598
- [5] Noell P J, Carroll J D and Boyce B L 2018 The mechanisms of ductile rupture *Acta Mater.* **161** 83–98
- [6] Schwartz J, Fandeur O and Rey C 2010 Fatigue crack initiation modeling of 316LN steel based on non local plasticity theory *10th Int. Fatigue Conf., Fatigue 2010 (Proc. Eng. vol 2) (Prague, Czech Republic, 06–11 June 2010)* ed P Lukas pp 1353–62
- [7] Takeno T, Wang P, Takagi T and Miki H 2013 Early fatigue damage detecting sensors review and prospects *Sensors Actuators A* **198** 46–60
- [8] Carroll J, Abuzaid W, Lambros J and Sehitoglu H 2010 An experimental methodology to relate local strain to microstructural texture *Rev. Sci. Instrum.* **81** 083703
- [9] Niendorf T, Dadda J, Canadinc D, Maier H J and Karaman I 2009 Monitoring the fatigue-induced damage evolution in

- ultrafine-grained interstitial-free steel utilizing digital image correlation *Mater. Sci. Eng. A* **517** 225–34
- [10] Benoit A, Remy L, Koester A, Maitournam H and Oger F 2014 Experimental investigation of the behavior and the low cycle fatigue life of a welded structure *Mater. Sci. Eng. A* **595** 64–76
- [11] Cesnik S J M and Boltezar M 2012 Uninterrupted and accelerated vibrational fatigue testing with simultaneous monitoring of the natural frequency and damping *J. Sound Vib.* **331** 5370–82
- [12] Kobayashi T, Muragishi O and Nihei K 2004 Development of fatigue detecting sensor *Advances in Fracture and Failure Prevention (Key Engineering Materials vol 261–263) ed ) ed K Kishimoto et al (Zurich, Switzerland: Trans Tech) pp 1313–8*
- [13] Ignatovich S R, Menou A, Karuskevich M V and Maruschak P O 2013 Fatigue damage and sensor development for aircraft structural health monitoring *Theor. Appl. Fract. Mech.* **65** 23–7
- [14] Hearn G and Testa R B 1991 Modal-analysis for damage detection in structures *J. Struct. Eng.—ASCE* **117** 3042–63
- [15] Li D, Ho S-C M, Song G, Ren L and Li H 2015 A review of damage detection methods for wind turbine blades *Smart Mater. Struct.* **24** 033001
- [16] Alavi A H, Hasni H, Jiao P, Borchani W and Lajnef N 2017 Fatigue cracking detection in steel bridge girders through a self-powered sensing concept *J. Constr. Steel Res.* **128** 19–38
- [17] Lee Y-J and Cho S 2016 SHM-based probabilistic fatigue life prediction for bridges based on FE model updating *Sensors* **16** 317
- [18] Boller C et al (ed) 2009 *Encyclopedia of Structural Health Monitoring* (New York: Wiley) (<https://doi.org/10.1002/9780470061626>)
- [19] Sbarufatti C, Manes A and Giglio M 2014 Application of sensor technologies for local and distributed structural health monitoring *Struct. Control Health Monit.* **21** 1057–83
- [20] Balageas D, Fritzen C-P and Güemes A 2010 *Struct. Health Monit.* vol 90 (New York: Wiley) (<https://doi.org/10.1002/9780470612071>)
- [21] Farrar C R and Worden K 2007 An introduction to structural health monitoring *Phil. Trans. R. Soc. A* **365** 303–15
- [22] Eickhoff W F and Ulrich R F 1981 Optical frequency domain reflectometry in single-mode fiber *Appl. Phys. Lett.* **39** 693–5
- [23] Soller B J, Gifford D K, Wolfe M S and Froggatt M E 2005 High resolution optical frequency domain reflectometry for characterization of components and assemblies *Opt. Express* **13** 666–74
- [24] Leal-Junior A, Theodosiou A, Diaz C, Marques C, Pontes M J, Kalli K and Frizera-Neto A 2018 Fiber bragg gratings in CYTOP fibers embedded in a 3D-Printed flexible support for assessment of human-robot interaction forces *Materials* **11** 2305
- [25] Monaghan T, Capel A J, Christie S D, Harris R A and Friel R J 2015 Solid-state additive manufacturing for metallized optical fiber integration *Composites A* **76** 181–93
- [26] Havermann D, Mathew J, MacPherson W N, Maier R R J and Hand D P 2015 Temperature and strain measurements with fiber bragg Gratings embedded in stainless steel 316 *23rd Int. Conf. on Optical Fibre Sensors (Santander, Spain, 02–06 June 2014); J. Lightw. Technol.* **33** 2474–9
- [27] Carroll B E, Palmer T A and Beese A M 2015 Anisotropic tensile behavior of Ti–6Al–4V components fabricated with directed energy deposition additive manufacturing *Acta Mater.* **87** 309–20
- [28] Stranza M 2016 *Additive Manufacturing as a Tool for Structural Health Monitoring of Metallic Structures* vol 1 (Zelzate: University Press)
- [29] Strantza M, De Baere D, Rombouts M, Maes G, Guillaume P and Van Hemelrijck D 2015 Feasibility study on integrated structural health monitoring system produced by metal three-dimensional printing *Struct. Health Monit.* **14** 622–32
- [30] Hinderdael M, De Baere D and Guillaume P 2018 Fatigue performance of powder bed fused Ti–6Al–4V component with integrated chemically etched capillary for structural health monitoring application *18th Int. Conf. on Experimental Mechanics (ICEM18) (https://doi.org/10.3390/ICEM18-05419)*
- [31] Hinderdael M, Strantza M, De Baere D, Devesse W, De Graeve I, Terryn H and Guillaume P 2017 Fatigue performance of Ti–6Al–4V additively manufactured specimens with integrated capillaries of an embedded structural health monitoring system *Materials* **10** 993
- [32] Kuang K S C, Quek S T and Maalej M 2004 Assessment of an extrinsic polymer-based optical fibre sensor for structural health monitoring *Meas. Sci. Technol.* **15** 2133–41
- [33] Capell T F, Palaniappan J, Ogini S L, Crocombe A D, Reed G T, Thorne A M, Mohanty L and Tjin S C 2007 The use of an embedded chirped fibre Bragg grating sensor to monitor disbond initiation and growth in adhesively bonded composite/metal single lap joints *Photon 2006 Conf. (Univ Manchester, Manchester, UK, 04–07 September 2006); J. Opt. A: Pure Appl. Opt.* **9** S40–4
- [34] De Pauw B, Lamberti A, Ertveldt J, Rezayat A, van Tichelen K, Vanlanduit S and Berghmans F 2016 Vibration monitoring using fiber optic sensors in a lead-bismuth eutectic cooled nuclear fuel assembly *Sensors* **16** 571
- [35] Luna Optical backscatter reflectometer OBR4600 specs: [lunainc.com/wp-content/uploads/2012/11/obr-4600-data-sheet-9-mar-2018.pdf](http://lunainc.com/wp-content/uploads/2012/11/obr-4600-data-sheet-9-mar-2018.pdf), 03-2018
- [36] Von Der Weid J P, Passy R, Mussi G and Gisin N 1997 On the characterization of optical fiber network components with optical frequency domain reflectometry *J. Lightwave Technol.* **15** 1131–41
- [37] Passy R, Gisin N and Von der Weid J-P 1995 High-sensitivity-coherent optical frequency-domain reflectometry for characterization of fiber-optic network components *IEEE Photonics Technol. Lett.* **7** 667–9
- [38] Hill W, Kübler J and Fromme M 2010 Single-mode distributed temperature sensing using OFDR *Proc. SPIE* **7653** 765342
- [39] Sang A K, Froggatt M E, Gifford D K, Kreger S T and Dickerson B D 2008 One centimeter spatial resolution temperature measurements in a nuclear reactor using rayleigh scatter in optical fiber *IEEE Sens. J.* **8** 1375–80
- [40] Yüksel K, Mégret P and Wuilpart M 2011 A quasi-distributed temperature sensor interrogated by optical frequency-domain reflectometer *Meas. Sci. Technol.* **22** 115204
- [41] Song J, Li W, Lu P, Xu Y, Chen L and Bao X 2014 Long-range high spatial resolution distributed temperature and strain sensing based on optical frequency-domain reflectometry *IEEE Photonics J.* **6** 1–8
- [42] Murayama H, Wada D and Igawa H 2013 Structural health monitoring by using fiber-optic distributed strain sensors with high spatial resolution *Photonic Sens.* **3** 355–76
- [43] Murayama H, Kageyama K, Uzawa K, Ohara K and Igawa H 2012 Strain monitoring of a single-lap joint with embedded fiber-optic distributed sensors *Struct. Health Monit.* **11** 325–44
- [44] Hollenberg G W, Terwilliger G R and Gordon R S 1971 Calculation of stresses and strains in four-point bending creep tests *J. Am. Ceram. Soc.* **54** 196–9